PROCEEDINGS, 49th Workshop on Geothermal Reservoir Engineering
Stanford University, Stanford, California, February 12-14, 2024
SGP-TR-227

The Rheology of Temperature-Responsive Volume-Phase Transition Hydrogels for the Improved Thermal Performance and Lifetime of Geothermal Reservoirs

Aaron M. Baxter[1], Danni Tang[2], Adam J. Hawkins[1], Ulrich B. Wiesner[2], Patrick M. Fulton[3], Christopher A. Alabi[1], Jefferson W. Tester[1], Sarah Hormozi[1]

Robert Frederick Smith School of Chemical & Biomolecular Engineering[1], Materials Science & Engineering[2], Earth & Atmospheric Sciences[3], College of Engineering, Cornell University, 113 Ho Plaza, Ithaca, NY 14850, USA.

amb639@cornell.edu

Keywords: premature thermal breakthrough, short circuit, hydrogel, yield stress, hydraulic control, viscosity.

ABSTRACT

A primary concern limiting the expansion of geothermal energy use throughout the world is the inherent risk of premature thermal breakthrough which occurs when production temperatures drop below values set by design/operating criteria earlier than anticipated. Production temperatures can rapidly drop due to "short circuits" or flow paths with insufficient stored thermal energy or heat transfer area. The risk of premature thermal breakthrough is not only difficult to predict, but with large capital investment requirements for geothermal systems, it can result in catastrophic economic failure. The use of temperature-responsive volume-phase transition (VPT) hydrogel suspensions presents an ability to effectively redirect flow around short circuit paths and increase heat transfer area by forming a yield stress fluid in colder short-circuited regions, ultimately improving the thermal performance and lifetime of geothermal systems through the formation of a yield stress fluid. In this paper, we demonstrate the ability of these hydrogels suspensions to form yield stress fluids along with establishing an empirical connection between the measured yield stress, the volume fraction, and temperature of the hydrogel suspension.

1. INTRODUCTION

Geothermal energy represents a major and largely untapped indigenous resource for nations to increase their energy security and lower their carbon emissions. Geothermal boasts many advantages to alternatives by being a baseload energy source, meaning its production is not intermittent or dependent on external conditions like wind or sunlight. It is also not dependent on the import of fossil fuel energy sources which can become easily disrupted in times of international stress. Through the use of enhanced geothermal systems, geothermal is now a viable option in many parts of the world, and not exclusive to regions with high surface heat flux or relatively shallow heat sources like that of the Western United States, Iceland, and more. Enhanced geothermal systems can make use of heat in relatively colder regions, particularly for direct use heating, which makes up a large portion of energy use in cold areas. However, a major drawback to geothermal energy is the uncertainty of the productivity of a well, as it relies heavily on subsurface modeling, simulation, and predictions. Combined with the hefty capital cost involved in drilling and characterization of a potential well, failure to meet production goals can lead to total economic failure of a well. One of the key modes of failure in geothermal systems is the formation of "short-circuits", which can lead to premature thermal breakthrough. This occurs when a path from the injector to producer-well has exceptional hydraulic performance but insufficient heat transfer area, reducing temperatures in that area rapidly. This results in a cold path or "short circuit", which drastically reduces the production temperature and output of a system and can lead to economic failure.

Previous reservoir simulations performed by Hawkins et al. (2023), demonstrated the impact a redistribution of flow could have on a short-circuited channel. The simulations used a numerical simulator introduced by Fox et al. (2015) to simulate the combined effects of rock conduction and advection in the case of a single planar fracture with a non-uniform aperture distribution. This fracture underwent a 1,000-meter flow from injector to producer-well. Mass flow rate, rock thermal conductivity, fluid density, and rock density were 20 kg/s, 2.5 W/m-K, 1000 kg/m^3, and 2,500 kg/m^3 respectively. The rock was assumed to have an initial temperature of 200 ^{o}C, while water is injected at 50 ^{o}C. When a node in the simulation dropped below 190 ^{o}C, indicating a short circuit, the aperture in this area was reduced by a factor of 40, redirecting flow around the short circuit. For more detailed information on this simulation please see Ref. 1 (Hawkins et al., 2023). These aperture changes substantially increased the desirable heat transfer area and reduced unnecessary thermal losses caused by short-circuits. Overall, the effect is an increase in production temperatures over increased timespans, significantly improving the lifetime and viability of the system. Figure 1 displays a fluid temperature map within the fracture after 30 years of continuous recirculation for a case without a change in aperture (pre-treatment) and a case with changes in aperture (post-treatment) (Hawkins et at., 2023).

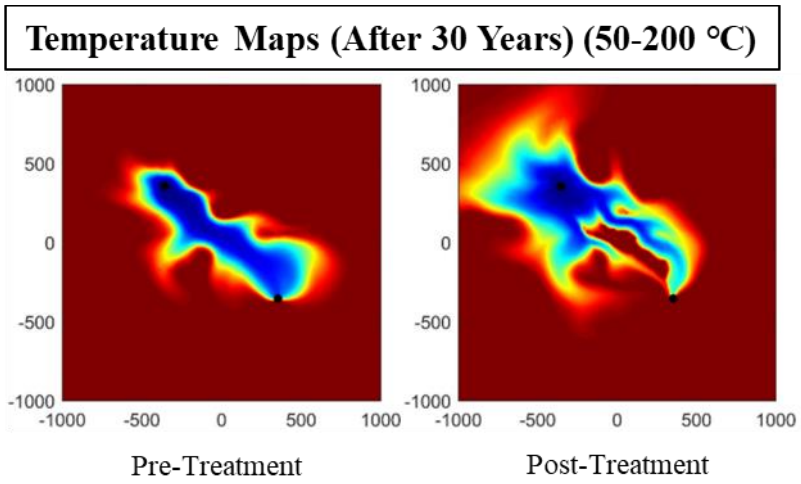

Figure 1: Fluid temperature after 30 years of continuous circulation for a pre-treatment (no changes in aperture) and post-treatment (adjustments in aperture) case. Spatial coordinates are in meters and the temperature ranges from 200 °C (dark red) to 50 °C (dark blue). The injector (top left) and producer (bottom right) wells are indicated by black dots (Hawkins et al., 2023).

For the pre-treatment case in Figure 1, a short circuit has formed between the injector and producer well, as there is a direct path between the wells at low temperature. In the post-treatment case, due to the formation of the short circuit, the aperture in the short-circuited region is reduced and flow is forced around it, increasing the heat transfer area. The result this has on the production well temperature is shown in Figure 2.

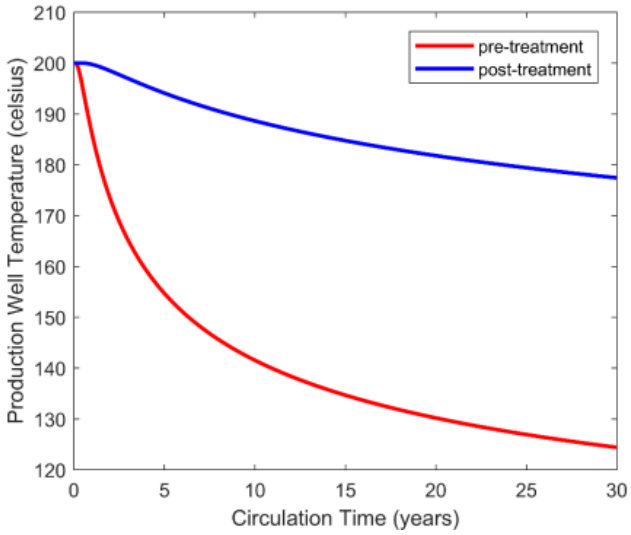

Figure 2: Production well fluid temperature vs time in years. Pre-treatment indicates a scenario of no aperture changes and no change in flow distribution. Post-treatment indicates the referenced aperture changes in which aperture is reduced by a factor of 40 in nodes where temperature dropped below 190 °C (Hawkins et al., 2023).

As a result of the change in aperture and increase in favorable heat transfer area, production temperatures for the post-treatment case are significantly higher over long periods of time. While adjustments in aperture distribution based on temperature are clearly a viable solution to the issues of short-circuiting, a real-world implementation does not currently exist. As a result of these simulations, we considered using temperature-responsive volume-phase transition (VPT) hydrogels as a practical solution to reduce and even close-off fracture apertures in undesirable "short-circuited" regions.

Volume-phase transition hydrogels are characterized by an abrupt and discontinuous change in their degree of swelling, transitioning from a closed "shrunken" state to a more open "swollen" state or vice versa. N-isopropylacrylamide (NIPA) hydrogels result from the polymerization of NIPA into a cross-linked network and have long been known for their counter-intuitive VPT properties, in which the hydrogel swells at low temperatures below a critical value and shrinks at temperatures above a critical value known as the lower critical solution temperature (LCST). NIPA hydrogels have been studied for decades and were ultimately pioneered by Toyoichi Tanaka in the

1970s and 1980s (e.g., Tanaka et al., 1979; Tanaka et al., 1985; Matsuo et al., 1988). The NIPA hydrogel is attributed to a pendant isopropylamide group, which induces a change in the hydrophilic-hydrophobic balance as the temperature changes.

The VPT can be more simply understood through the following mechanism: NIPA is a slightly hydrophobic polymer, but at low temperatures, water molecules are able to form cage-like structures around the individual polymer chains within the cross-linked network. This structure is able to screen any hydrophobic interactions between polymers, resulting in a more swollen and expanded network. However, at high temperatures, the water molecules are much more mobile and the cage-like structure begins to break down. At a certain threshold temperature, the hydrophobic interaction dominates and the network collapses on itself into a shrunken state.

In addition to the VPT properties of NIPA, Tanaka shows the copolymerization of NIPA with sodium acrylate (SA) to form pNIPA-SA gels can increase the temperature at which the VPT occurs. This is shown in Figure 3 (Tanaka et al., 1993). Ultimately, this provides a critical control parameter as the lower critical solution temperature can be controlled and adjusted based on the desired production temperatures of a specific geothermal system. It can also be seen that as the concentration of sodium acrylate is increased, the volumetric swelling ratio associated with the VPT increases.

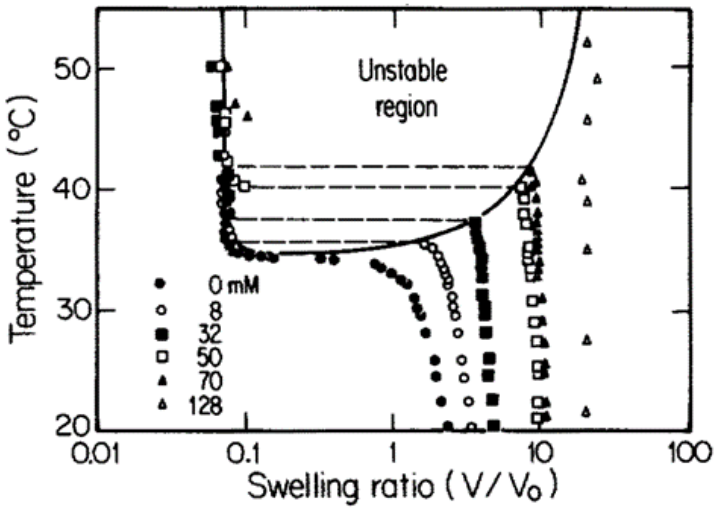

Figure 3: Plot of swelling ratio vs temperature for a variety of pNIPA-SA hydrogels. The legend displays the concentration of sodium acrylate (SA) while the overall monomer concentration of the hydrogels (NIPA + Sodium acrylate) was held constant at 700 mM. N,N'-Methylenebis(acrylamide) is held at 81 mM (Tanaka et al., 1993).

The kinetics of the VPT are primarily diffusion controlled. Although a bit counterintuitive, the process is not limited by the diffusion of the water molecules but rather that of the polymer matrix itself. This is well documented by Tanaka et al. (1988) in which he describes the kinetics following a single exponential decay with a diffusion coefficient known as the collective diffusion coefficient. For simplification in this paper, while the exact kinetic path for swelling versus shrinking is not the same, the overall time required to reach steady state for the two processes is almost identical as shown by Tanaka et al. (1988), as such we can assume a single effective diffusion coefficient can be used to represent both cases. This diffusion coefficient leads to a characteristic time of swelling or shrinking which is proportional to the square of the particle's radius over the diffusion coefficient:

$$\tau = \frac{R^2}{\pi^2 D} \tag{1}$$

where τ is the characteristic time of swelling or shrinking, R is the radius of the particle, and D is the collective diffusion coefficient.

The exact value of the collective diffusion coefficient is dependent on the temperature as shown by Tanaka et al. (1988), but for simplification, we can assume a commonly reported value for NIPA gels of 2-3.2 * 10^{-7} cm^2/s (Shibayama et al., 1999; Tanaka et al., 1979).

2. RESEARCH HYPOTHESIS

Ultimately, the technical objective is to utilize the VPT properties of a large number of NIPA-SA hydrogel particles to swell and jam a short-circuited fracture or channel whose temperature is below a designed lower critical solution temperature. We hypothesize that NIPA-SA hydrogel particles hold the potential to do this as when they are highly concentrated and grow through their VPT, they can drastically increase the volume fraction of the system and plug a fracture aperture. In order to fully plug and stop flow in an area, rather than simply reducing flow, the suspension must form a yield stress. A yield stress fluid is a material upon which any stresses applied less than the magnitude of the yield stress, elicits a solid response, but stresses greater than the yield stress elicits plastic deformation and causes the material to flow like a liquid. By generating a yield-stress fluid which exceeds the shear stresses within the channel, a solid plug is formed which is capable of redirecting flow around that area. A schematic is shown in Figure 4, in which the hydrogel suspension goes from a

non-yield stress material to a yield stress material through its VPT due to a reduction in temperature below the designed lower critical solution temperature. Fracture aperture and particle size varies, as such the schematic is not necessarily to scale.

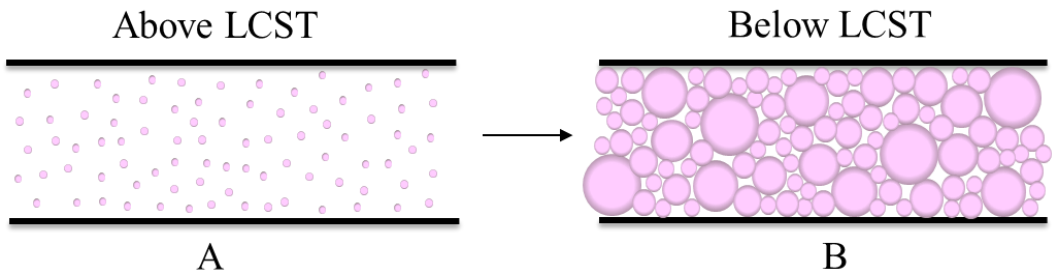

Figure 4: Schematic of the volume-phase transition within a fracture or channel. The material begins at a high or desirable temperature above the lower critical solution temperature (LCST) in state A. State B simulates a short circuit, where temperature drops below the lower critical solution temperature, inducing a VPT, jamming the fracture as the suspension forms a yield stress. Schematic is not to scale.

The hypothesis that NIPA-SA particles can form a yield stress fluid at high volume fractions is not a trivial one. Although many yield stress systems have been studied such as high-volume fraction suspensions and emulsions, none involve the particles readily exchanging fluid/mass with the suspending fluid. We predict that despite this, by exceeding the jamming volume fraction with NIPA-SA particles, a yield stress fluid can be formed regardless, primarily due to the deformation of particles and stored elastic energy. With rigid, mono-sized particles in a randomly packed configuration, the jamming volume fraction is about 0.64. However, working with hydrogel suspensions, this number can be much larger due to deformability and polydispersity. To design an effective solution, characterization of the yield stress of these suspensions is crucial.

The characterization of yield stress fluids is typically performed by a rheometer, which can give detailed information on many fluids and solids. This is primarily completed by shearing the fluid to form a simple shear flow and controlling or measuring important quantities to gather information on the material. This can be done in many configurations but the simplest is a parallel plate system in which a circular top plate spins and shears a material in a gap contained by a non-rotating bottom plate. Fundamentally, a rotational rheometer functions by applying and measuring torque and angular displacement/velocity. With this information and assumptions of no-slip at the boundaries and simple shear flow, parameters such as shear stress, shear rate, viscosity, and much more can be calculated giving critical information on the sample.

Analogous to the schematic in Figure 4, we hope to see the formation of a yield stress fluid at low temperatures below the lower critical solution temperature, but also a reversible elimination of the yield stress when the temperature is above the lower critical solution temperature. This formation and elimination of the yield stress is fully controlled by the volume fraction of the system, which is inherently coupled with the temperature of the system. Ideal rheological results displaying the hypothesized formation and elimination of the yield stress are shown in a schematic in Figure 5. States A and B correspond to states A and B shown in Figure 4.

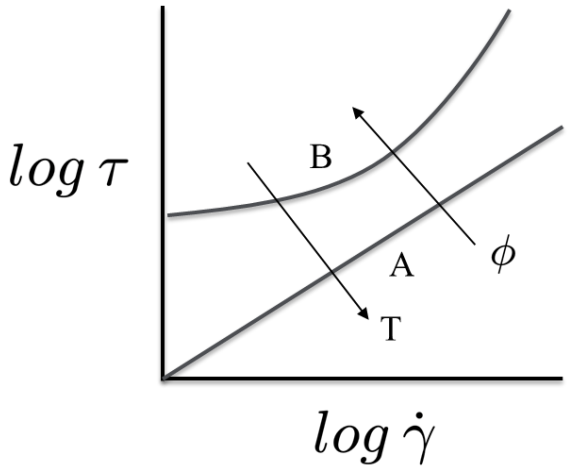

Figure 5: Schematic of the expected change is a shear rate ($\dot{\gamma}$) vs shear stress (τ) plot during a VPT. At low temperature (state B), below the lower critical solution temperature, the volume fraction is maximized and the sample exhibits a yield stress. Above the lower critical solution temperature (state A), volume fraction lowers and the material no longer possesses a yield stress.

The shear stress is the stress applied to the material in order to achieve a specified shear rate. A shear rate is defined by the velocity of the top plate divided by the gap distance, yielding a value with units s^{-1}. The viscosity of a fluid is simply the shear stress divided by the shear rate. In Figure 5, we can see that in case A, where the suspension is at high temperature and low volume fraction, the shear stress goes to 0 as the shear rate goes to 0. However, in case B, when the suspension is above the jamming volume fraction, the shear stress plateaus and approaches a finite value as the shear rate goes to 0. This value is the yield stress of the suspension, as it is the minimum stress required to plasticly deform the suspension, meaning any stress applied lower than this value would result in zero shear rate or in other words, a solid response. Shear stress vs shear rate data is often fit to a Herschel-Bulkley model, a commonly used model for non-Newtonian continuum fluids due to its ability to describe some of the key components of a non-Newtonian fluid including the magnitude of its yield stress and shear-thinning or shear-thickening index. A Newtonian fluid is one whose viscosity is not affected by shear rate, while a non-Newtonian fluid does not follow Newton's laws of viscosity, meaning it can have a shear rate-dependent viscosity, possess a yield stress, or have time-related viscosity effects. The Herschel-Bulkley model is shown in Equation 2:

$$\tau = \tau_y + K\dot{\gamma}^n \tag{2}$$

where τ is the shear stress, τ_y is the yield stress, K is a consistency index, $\dot{\gamma}$ is the shear rate, and n is the flow index which indicates if the material is shear-thickening or thinning, which describes how the viscosity changes with shear rate.

While a rheometer is critical for measurements of yield stress and viscosity, it creates a simple shear flow, which differs from the channel flow which would be experienced by the suspension in a real sub-surface scenario. In a channel-flow, the shear stress is zero at the center of the channel, and increases linearly until it reaches a maximum at the walls, in this case the rock-surface. Assuming a 2-D planar fracture in a real subsurface system, this can be further simplified to a 1-D channel flow, where the direction of flow is in the z-direction and the aperture is characterized by the y-direction. With knowledge of the fracture aperture and applied pressure gradient, we can characterize the shear stress in the channel.

$$\tau_{yz} = \frac{1}{2}\frac{dP}{dz}y \tag{3}$$

where τ_{yz} is the shear stress, y is the distance from center perpendicular to the direction of flow, z is the direction of flow, and P is the pressure. A schematic of this is shown in Figure 6.

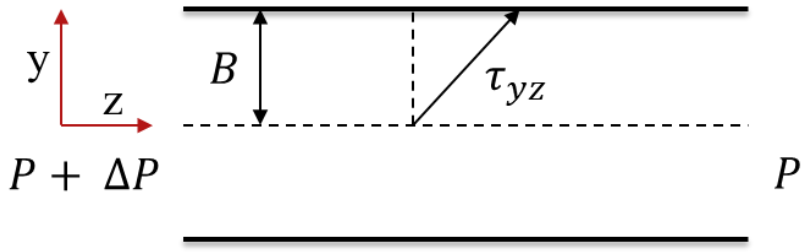

Figure 6: Schematic of the shear stress within a 1-D channel flow in a fracture due to a pressure-driven flow. Shear stress increases linearly in the y-direction until it reaches a maximum at the wall.

A nondimensionalized yield number can be extracted by rearranging Equation 1 and replacing τ_{yz} with τ_y and y with B such that a comparison can be made between the yield stress and the maximum shear stress at the wall, as shown in Equation 4.

$$Y = \frac{2\tau_y}{\frac{dP}{dz}B} \tag{4}$$

where τ_y is the yield stress and B is the distance from center to the wall such that the total aperture is equal to $2B$. It can be noted that when Y is equal to 1, the yield stress is equal to the shear stress at the wall, and therefore the entire fluid behaves as a solid and plugs the flow. If Y is greater than 0, meaning the suspension has a yield stress, but is less than 1, we observe a solid region in the center of the channel where shear stresses are low, surrounded by a liquid region in the annulus where the shear stress exceeds the yield stress. This can be visualized in Figure 7 in which a Herschel-Bulkley fluid was modeled for a 1-D channel flow where the yield stress is varied to achieve a variety of yield numbers, consistency and flow index are 1 Pa*s and 1 respectively, B is 2.5 mm, and a pressure gradient of 10 kPa/m is applied.

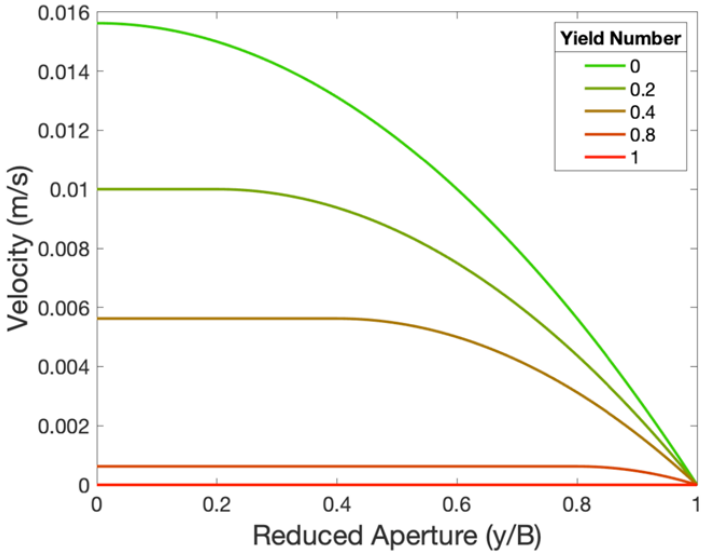

Figure 7: Herschel-Bulkley modeling of 1-D channel flow expressing flow velocity as a function of reduced aperture for a variety of yield numbers. Pressure gradient, aperture, flow index, and consistency index are held constant as described. A reduced (non-dimensional) aperture of 0 indicates being in the center of the channel of aperture 2B, while a reduced aperture of 1 indicates being at the wall.

3. SYNTHESIS AND CHARACTERIZATION

3.1 Synthesis

The introduction of sodium acrylate in the hydrogel synthesis measurably changes the hydrogel's properties, including that of the swelling ratio and lower critical solution temperature. However, we move beyond the work performed by Tanaka and control the mechanical and detection properties of the particles through changes in synthesis.

Cross-linked pNIPA-SA hydrogels are prepared through free-radical polymerization of NIPA and sodium acrylate in the presence of an organic cross-linker N,N'-Methylenebis(acrylamide) (BIS) and natural clay cross-linkers Laponite RD or Laponite RDS. Samples are made in proportions such that they make 20 mL of aqueous solution and NIPA-SA concentrations are held such that their total concentration is equal to 700 mM. Tetramethylethylenediamine is used as an accelerator in the amount of 37.36 mg. Ammonium persulfate is used as an initiator at 3.5 mM. The concentration of organic and natural cross-linkers varies based on recipe. Rhodamine B is also added at 1 mg to allow fluorescence detection of particles.

The mechanical properties of pNIPA-SA hydrogels can be controlled through the degree of cross-linking in the gel. This is done via organic cross-linking with N,N'-Methylenebis(acrylamide) or through natural cross-linking with Laponite RD and Laponite RDS clays. Both methods have been previously demonstrated to improve both the shear modulus (G) and Young's modulus (E) of the hydrogels (Xu et al., 2015; Haraguchi et al., 2007). Simulations of suspensions of deformable viscoelastic spheres have suggested that as the shear modulus increases, the jamming volume fraction decreases, ultimately reducing the volume fraction required to jam a system (Rosti et al., 2018). However, increasing the shear modulus through an increase in the cross-link density inherently decreases the swelling ratio of the gel, which is highly undesirable. The introduction of clays could also lead to possible adhesion between particles which could serve beneficial. Ultimately, a variety of recipes of pNIPA-SA gels must be well-understood to determine the most advantageous properties and optimum recipe to form a yield-stress fluid at the desired temperatures. This will likely involve a balancing of mechanical strength with swelling ratio through changes in the concentration of organic and natural cross-linkers. A comprehensive analysis of the mechanical properties of the produced pNIPA-SA gels is not included in this paper and will be included in future work.

Currently, pNIPA-SA hydrogels are synthesized via inverse suspension polymerization in which the aqueous solution is prepared as specified above, but without the accelerator. The aqueous solution is dispersed in a large volume of paraffin oil and sheared at a high rate with a mixing rod such that an emulsion is formed, at which point the accelerator is added and the polymerization occurs. This allows the formation of spherical hydrogel particles, but results in a highly polydisperse particle size distribution. Following the polymerization, the hydrogel particles are washed and removed from the paraffin oil and are left submerged in excess DI water for about 7 days to ensure they are fully swollen, realistically the time-scale required to fully swell is on the order of a couple hours or less. Once fully swollen, a particle size distribution can be determined through the use of a FlowCam device, a flow imaging device which visualizes a narrow channel of flow and automatically captures particles, giving many detailed statistics including size distribution. Flowcam utilizes a variety of flow cells or channel widths and with careful backlighting and constant imaging, recognizes when a particle is in view as it obstructs the background lighting. The size distribution for a particular recipe is shown below in Figure 8, in which roughly 1,400 fully swollen particles were imaged. A mean value of 250 microns was determined with a modal around 200 microns.

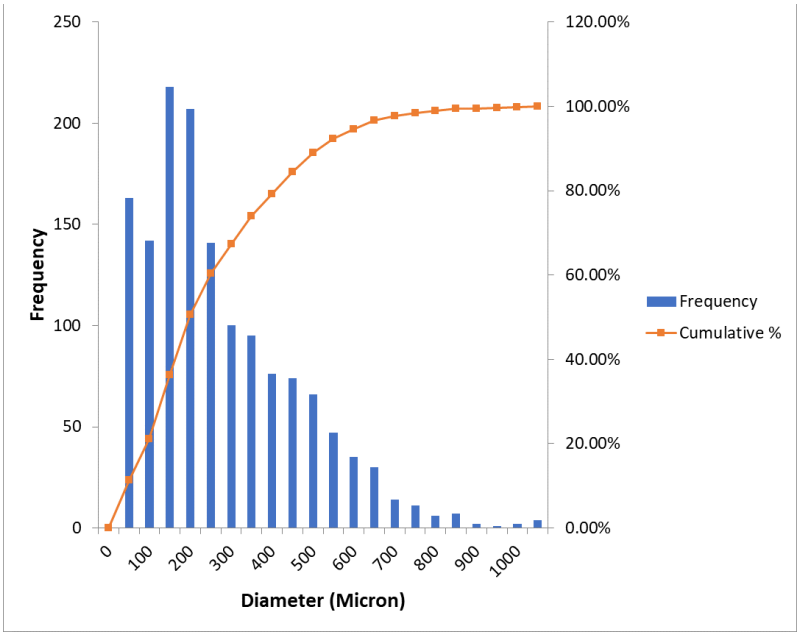

Figure 8: Particle size distribution of a pNIPA-SA recipe with 14.99 g/L Laponite RDS, 0.65 g/L BIS, and a 90:10 NIPA-Sodium acrylate ratio.

Volume fraction is a critical parameter of any particle suspension. In the dilute regime, we expect the suspension to behave hydrodynamically similar to water. At high temperatures, pNIPA-SA particles are in their shrunken state and minimize the volume fraction, ideally yielding a suspension with properties close to that of pure water at the same temperatures and pressures. At low temperatures, particles should swell to the extent that the volume fraction increases to the jamming volume fraction upon which the viscosity diverges and a yield stress fluid is formed. However, the precise volume fraction within the system is difficult to determine. This is primarily due to the fact that the volume fraction can readily change due to changes in the hydrogel's environment and they can absorb or desorb the fluid they are suspended in. A more precise way of measuring the volume fraction through visualization techniques is currently being developed in our lab, but for now we use a simple yet only approximate basis as described. Following the synthesis and swelling of the hydrogel particles, they are subsequently filtered under vacuum to remove interstitial water. Samples can then easily be weighed to make suspensions of particular mass ratios when combined with water. These mass ratios should be roughly similar to the volume fraction since the hydrogel particles are primarily composed of water when fully swollen, therefore having a similar density to that of pure water.

Imaging of the particles throughout their VPT has also been done via microscopy and fluorescence detection. The particle is placed in view and the surrounding temperature is jumped above the lower critical solution temperature such that the VPT is induced. This can be seen in Figure 9.

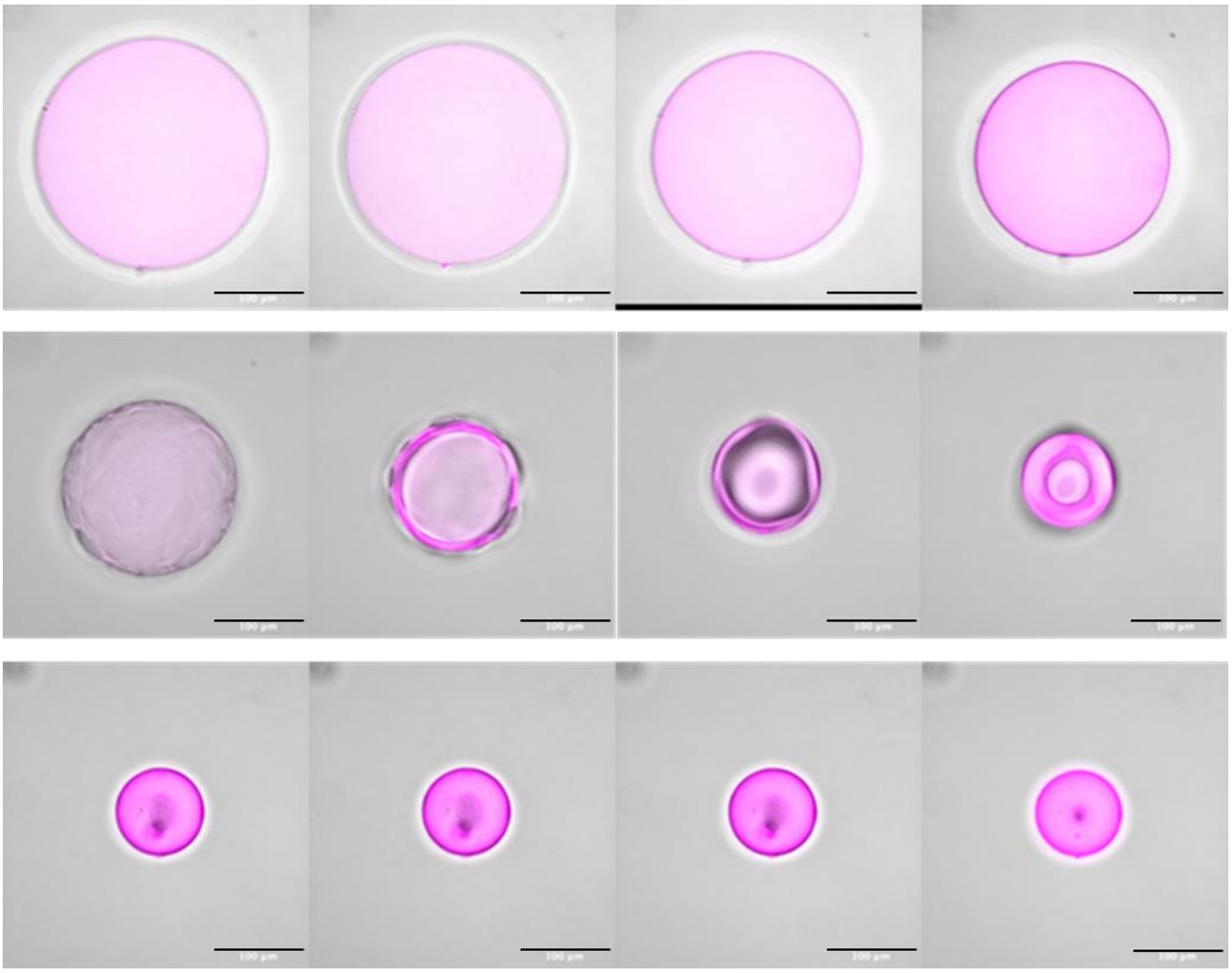

Figure 9: Visualization of a shrinking pNIPA-SA particle as the temperature is rapidly increased from below to above particle's LCST. Scale bar is 100-micron, series of pictures in time from left to right beginning at top left. Superimposed gray-scale and fluorescence detection.

The specific temperatures in Figure 9 at the time of each photograph are not precisely known but the overall series of images demonstrate the transition state of these materials from a swollen (low temperature) to a shrunken (high temperature) state.

3.2 Rheological Characterization

Rheology is performed via a stress-controlled Discovery HR30 rheometer using a TA 40 mm diameter crosshatched parallel plate (crosshatch patterns 1 mm across and 0.5 mm depth) geometry to eliminate slip. Temperature is controlled via lower Peltier plate. In this paper, yield-stress and viscosity vs temperature for a variety of volume fractions and recipes provide critical information for determining an optimum recipe.

A rheological study of a particular recipe demonstrates the existence of yield stress in these materials and how it can be eliminated by lowering the volume fraction through dilution in Figure 10. As mentioned previously, volume fraction is difficult to accurately measure with current methods and as such, a mass fraction is used instead. The sample begins at a mass ratio of 1, meaning only particles post vacuum filtration are placed in the rheometer but are diluted as the mass fraction lowers. Each point (open circle) in Figure 10 represents an individual experiment in which the shear rate is held constant and the shear stress is monitored over time until it has reached a steady-state value. The testing begins at a gap of 1.5 mm and increases as the sample is diluted, going up to a gap of 3.24 mm at the lowest mass fraction. The data for each mass fraction has subsequently been fitted with a Herschel-Bulkley model.

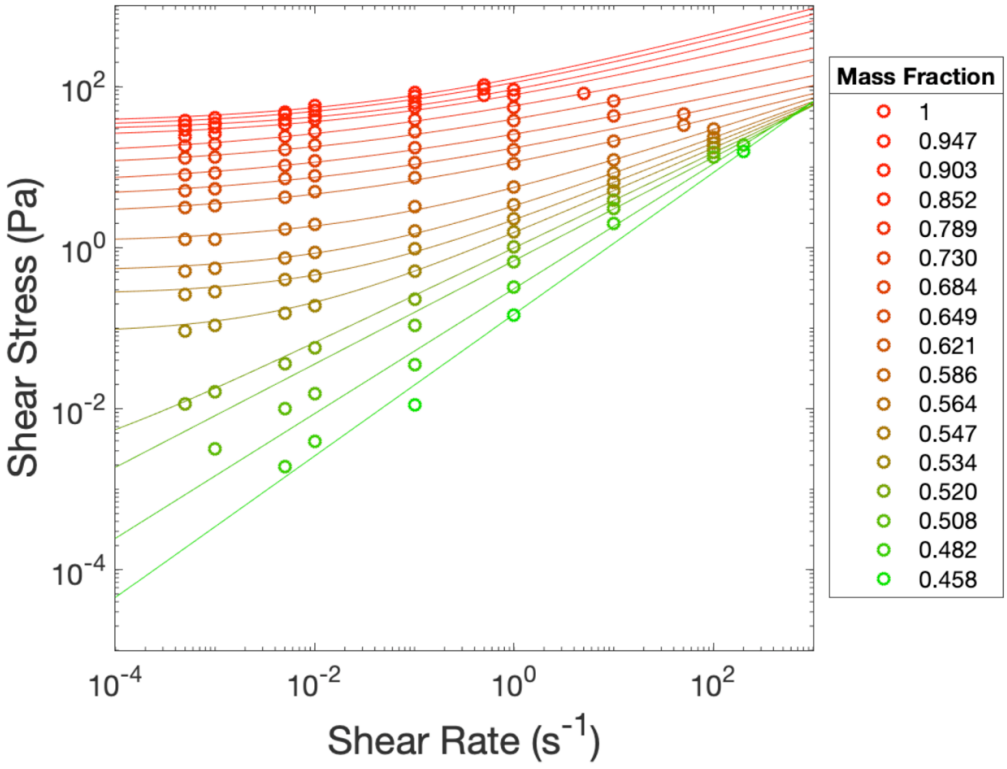

Figure 10: Log-log plot of shear stress vs shear rate at a variety of mass fractions for a pNIPA-SA particle suspension with no clay, 1.29 g/L BIS, and a 90:10 NIPA to SA ratio.

As expected for a soft deformable system such as this, the pNIPA-SA system is shear thinning, meaning the viscosity decreases as a function of shear rate. We can also estimate the yield stress of the material which can be estimated by the plateauing value at low shear rates. The yield stress is defined by the minimum stress required for the material to plasticly deform and flow like a liquid, so as the shear rate approaches the limit of 0, we are observing the minimum stress required to flow the material, giving an estimation of the yield stress. At a mass fraction of 1, the yield stress of this recipe is roughly 35 Pa. This provides clear evidence and supports our hypothesis that the pNIPA-SA particles are capable of forming a yield stress fluid. As the mass fraction and correspondingly the volume fraction is lowered through dilution, it can be seen that the yield stress decreases up until the point that there is no longer a plateau and the shear stress approaches 0, thereby eliminating all of the yield stress as the volume fraction goes below the jamming fraction.

The reduction and eventual elimination of the yield stress through dilution is analogous to the goal of eliminating the yield stress through changes in temperature and inducing a VPT. This effect is qualitatively shown in Figure 5, but in this case, the decrease in volume fraction is caused by dilution rather than a change in temperature

Figure 10 illustrates quantitatively the effect of dilution on yield stress. Importantly, gap dependency issues arise due to large particles within the gap as a result of the high polydispersity. To reduce the effects of gap dependency, monodisperse pNIPA-SA systems are currently being developed for rheological characterization, utilizing a specially designed optical rheology apparatus to more closely understand the effects of shear on the system.

As we understand the ability of pNIPA-SA particles to readily change their volume fraction with temperature, we can perform further rheological characterization to demonstrate how viscosity changes with temperature. In this case, a sample with a pNIPA-SA ratio of 90:10 is introduced at roughly mass fraction 1 and sheared at a constant shear rate of 5 s^{-1}. The sample begins at 25 ^oC and is ramped up to 80 ^oC at a rate of 2 ^oC/min. This rate was chosen to ensure the particles had reached their steady-state volume at each temperature during the measurements. A solvent trap filled with DI water is included to reduce evaporation although some evaporation does occur through the course of the test.

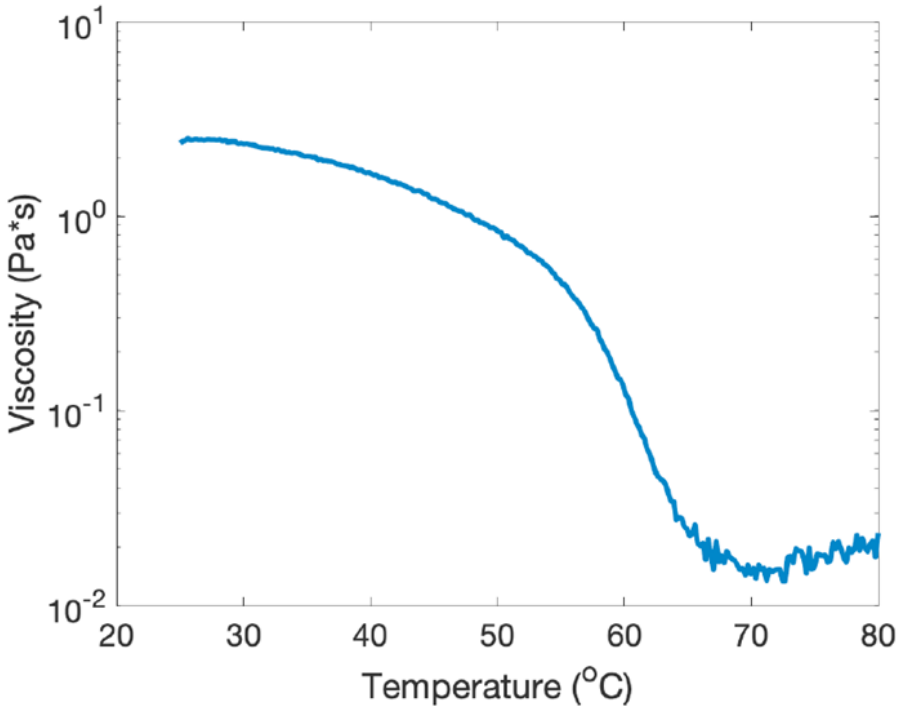

Figure 12: Temperature ramp in which temperature is increased at a constant value while viscosity is monitored. pNIPA-SA particle suspension with no clay, 1.29 g/L BIS, and a 90:10 NIPA to SA ratio.

As seen in Figure 12, the suspension viscosity begins at a large value around 2.5 Pa*s at 25 °C. This viscosity is several orders of magnitude higher than that of pure water which has a viscosity of $8.89 * 10^{-4}$ Pa*s at the same temperature. As temperature is increased, the viscosity slowly falls until the point at which it hits its lower critical solution temperature and the VPT occurs somewhere around 50 - 60 °C. While the yield stress is unknown at each data point in this type of test, since the temperature and volume fraction are coupled, it can be interpreted that at low temperature, the material possesses a yield stress which is subsequently eliminated as the material is heated and the volume fraction decreases. As a result of this decrease in volume fraction, we can see a decrease in viscosity by about 2 orders of magnitude. Improvements to this test are planned to limit evaporation at high temperatures and determine the effects of particle settling within the rheometer gap.

4. CONCLUSIONS

Geothermal "short-circuits" present a large risk to investment in geothermal development because they significantly reduce reservoir performance. Being able to lower geothermal short circuiting by redistributing the fracture aperture will increase the productivity and lifetime of fractured well systems. The use of pNIPA-SA hydrogel particles which can change size in response to temperature changes offers the possibility to limit the negative effects of cold short circuits by acting as a practical means to redistribute the fracture aperture. If successfully deployed, these hydrogels have the potential to revolutionize the geothermal industry by providing a means to improve thermal performance throughout a geothermal reservoir's production period.

This paper demonstrates the capability of pNIPA-SA particle suspensions to form a yield stress fluid at temperatures below a designed lower critical solution temperature (LCST). At warmer temperature above the lower critical solution temperature, the yield stress is effectively eliminated and results in a fluid phase with a much lower viscosity. Ideally, these particles would be injected in pulses such that any short-circuits in the system can be plugged while any particles that do not plug and continuously flow through the reservoir can be subsequently filtered out to eliminate any increases in viscosity associated with the shrunken particles.

In future work, a comprehensive analysis of the mechanical properties of each recipe of pNIPA-SA particles will be conducted to understand the effect of mechanical properties on yield stress and jamming capabilities. Improvements to rheological measurements will also be completed, primarily focused on the synthesis of monodisperse suspensions to improve the understanding of the system then working out to polydisperse systems. Characterization of adhesion between particles is also planned as adhesion between particles could be a highly beneficial attribute to the ability of the particles to more effectively form a localized flow restriction within the reservoir. Lastly, implementation of visualization techniques to perform optical rheology are currently being developed and will be introduced to gain a full understanding of the behavior of these systems.

Ultimately, through rheological characterization and the use of bench-scale apparatus, we aim to identify "optimum" recipes which can be produced in greater quantities for large-scale testing. This can be performed in field sites such as the well-characterized Altona field site in Upstate NY or through the planned development of a large-scale model system.

ACKNOWLEDGEMENTS

This material is based upon work supported by the U.S. Department of Energy's Office of Energy Efficiency and Renewable Energy (EERE) under the Geothermal Technologies Office, Award Number DE-EE0009786. The views expressed herein do not necessarily represent the view of the U.S. Department of Energy or the United States Government.

REFERENCES

A. Hawkins et. al. "Active Tracers for Hydraulic Control of Cooled Short Circuits". (2023).

Di Xu, Divya Bhatnagar, Dilip Gersappe, Jonathan C. Sokolov, Miriam H. Rafailovich, and Jack Lombardi. Macromolecules 2015 48 (3), 840-846.

Eriko Sato Matsuo, Toyoichi Tanaka; Kinetics of discontinuous volume–phase transition of gels. J. Chem. Phys. 1 August 1988; 89 (3): 1695–1703.

Fox, D. B., Koch, D.L., and Tester,J. W.: The Effect of Spatial Aperture Variations on the Thermal Performance of Discretely Fractured Geothermal Reservoirs, Geothermal Energy, 3, (2015).

Gilbert, D. Role of Adhesive and Friction Contacts in the Rheology of Non-Brownian suspensions (2021).

Kazutoshi Haraguchi and Liyuan Song. Macromolecules 2007 40 (15), 5526-5536.

Madraki Y, Hormozi S, Ovarlez G, Guazzelli E, Pouliquen O (2017). Enhanced Shear Thickening. Phys Rev Fluids 2(3):033301.

M. E. Rosti, L. Brandt, and D. Mitra, Rheology of suspensions of viscoelastic spheres: Deformability as an effective volume fraction, Phys. Rev. Fluids 3, 012301 (2018).

Ovarlez, G., & Hormozi, S (Eds.). (2019). Lectures on visco-plastic fluid mechanics. Springer International Publishing.

Shibayama, M., Nagai, K. (1999). Shrinking Kinetics of Poly(N-isopropylacrylamide) Gels T-Jumped across Their Volume Phase Transition Temperatures. Macromolecules 1999, 32, 7461-7468.

Shibayama, M., Tanaka, T. (1993). Volume phase transition and related phenomena of polymer gels. In: Dusek, K. (eds) Responsive Gels: Volume Transitions I. Advances in Polymer Science, vol 109. Springer, Berlin, Heidelberg.

Tanaka T, Sato E, Hirokawa Y, Hirotsu S, Peetermans J. Critical kinetics of volume phase transition of gels. Phys Rev Lett. 1985 Nov 25;55(22):2455-2458.

Toyoichi Tanaka, David J. Fillmore; Kinetics of swelling of gels. J. Chem. Phys. 1 February 1979; 70 (3): 1214-1218.